Quaternary Science Reviews 301 (2023) 107939

Contents lists available at ScienceDirect

Quaternary Science Reviews

journal homepage: www.elsevier.com/locate/quascirev

Fluvial responses to late Holocene hydroclimate variability in the midcontinental United States

Maxwell N. Wright [a], Broxton W. Bird [a, b, *], Derek K. Gibson [a], Harvie Pollard [a], Jaime Escobar [c, d], Robert C. Barr [a, b]

[a] Department of Earth Sciences, Indiana University-Purdue University, Indianapolis, 46202, USA
[b] Center for Earth and Environmental Sciences, Indiana University-Purdue University, Indianapolis, 46202, USA
[c] Universidad del Norte, Barranquilla Colombia, Km 5 Via Puerto Colombia, Barranquilla, Colombia
[d] Center for Tropical Paleoecology and Archaeology, Smithsonian Tropical Research Institute, Box 0843-03092, Balboa, Panama

ARTICLE INFO

Article history:
Received 20 October 2022
Received in revised form
19 December 2022
Accepted 20 December 2022
Available online 5 January 2023

Handling editor: Claudio Latorre

Keywords:
Medieval climate anomaly
Little ice age
Fluvial geomorphology
Flood frequencies
Climate-flood relationships
Paleoclimatology

ABSTRACT

Long-term relationships between mean-state climatic conditions and flood frequencies in the midcontinental United States (US) are not well established because instrumental records of fluvial processes are limited to the current warm period (CWP; the last ca. 150 years) and continuous paleo-flood records are exceedingly rare. Here, we investigate climate-flood relationships in the midcontinental US by reconstructing flood frequencies at Half Moon Pond, a 1600-year-old oxbow lake on the lower White River, Indiana (watershed = ca, 29,000 km^2). We used sediment accumulation rates and clastic fluxes constrained by high-resolution radiocarbon (^{14}C) dating. Frequent flooding, as indicated by high sedimentation rates and clastic fluxes to Half Moon Pond, occurred leading up to and during the Medieval Climate Anomaly (MCA; 950–1250 CE) when paleoclimate records suggest the predominance of ocean-atmosphere mean states resembling the negative phases of the Pacific Decadal Oscillation (-PDO-like) and Pacific North American Mode (-PNA-like). Reductions in sedimentation rates and clastic fluxes, indicating reduced flooding, subsequently occurred during the transition out of the MCA and into the Little Ice Age (LIA; 1250–1830 CE) as ocean-atmosphere conditions shifted to + PDO-like and +PNA-like mean states. Sedimentation rates and clastic fluxes increased again after ca. 1800 CE, indicating increased flooding during the CWP as ocean-atmosphere conditions returned to -PDO-like and -PNA-like mean states. The White River trends were notably antiphased with sedimentation-rate-based flood frequencies for the lower Ohio River (500,000 km^2 watershed) prior to 1830 CE. This antiphased relationship is consistent with flooding in moderate to small watersheds in the Midwest being sensitive to the occurrence of rainstorm events, which were more frequent leading up to and during the MCA, and flooding in large watersheds being more sensitive to large spring melts associated with extensive snowpacks, which characterized the LIA. That both the White and Ohio rivers experienced their most frequent flooding during the CWP suggests deforestation and changing land use practices increased flooding on Midwestern watersheds across scales despite a current climatic mean state that in the past only resulted in increased flooding on moderate to small watersheds. Continued increased in midcontinental rainfall are therefore likely to enhance the occurrence of floods in Midwestern watersheds across different geographic scales.

1. Introduction

Recent increases in flood frequency, duration, and, in some cases, magnitude in the Midwestern United States (US) has spurred interest in climate-fluvial relationships and their response to changing climatic conditions (e.g., Mallakpour and Villarini, 2015; Xiao et al., 2013). Determining climate-flood relationships requires long, continuous discharge records from natural streams to ensure that their discharge variations reflect natural climatic and not anthropogenic signals. But even the longest instrumental records

* Corresponding author. Department of Earth Sciences, Indiana University-Purdue University, Indianapolis, 46202, USA.
E-mail address: bwbird@iu.edu (B.W. Bird).

https://doi.org/10.1016/j.quascirev.2022.107939
0277-3791/

from US streams determined to be the least impacted by human activities are restricted to the last ca. 100 years (Lins, 2012; Slack et al., 1993). From a paleoclimatic perspective, the last 100 years is part of the current warm period (CWP; last ca. 150 years), which has been characterized by generally consistent climate with mild winters and extended warm seasons with ample rainfall in the Midwestern US (Bird et al., 2017). It is therefore not possible to evaluate the role of mean state climate shifts on fluvial dynamics. Additionally, extensive land clearance during the last 150 years (Greeley, 1925) additionally means that even streams considered natural today exist within a fundamentally altered landscape. Climate-fluvial relationships under "natural" conditions and the impact of anthropogenic activities on climate-fluvial dynamics therefore remains uncertain.

Natural archives that preserve proxy records of climatic conditions and fluvial processes are required because instrumental records lack the temporal length to investigate long-term climate-fluvial relationships. An increasing number of paleoclimate records from the North American midcontinent document significant mean state climate changes during the last 2 millennia (2 ka) that lasted from decades to centuries. Prominent among these climatic events were the Medieval Climate Anomaly (MCA; 950–1250 CE) and Little Ice Age (LIA; 1350–1850 CE) (Bird et al., 2017; Mann et al., 2009). Similar to today, the MCA in the Midwest was characterized by extended warm-season (April–October) conditions with ample rainfall from the Gulf of Mexico and mild winters with limited moisture from the North Pacific and Arctic (Bird et al., 2017; Pompeani et al., 2021). The LIA was conversely characterized by cool conditions in the Midwest with decreased warm-season and increased cold-season (November–March) precipitation (i.e., snowfall) sourced from the North Pacific and/or Arctic (Bird et al., 2017; Pompeani et al., 2021).

Fluvial responses to seasonal precipitation shifts during the MCA and LIA are not well known because records documenting these processes are limited. Determining fluvial responses during the MCA and LIA is important because they offer a natural test of how fluvial systems responded to seasonal changes in precipitation prior to the extensive Euro-American deforestation and land use changes starting in the 1700s (Greeley, 1925). A 3000-year-long flood frequency reconstruction from Avery Lake on the lower Ohio River (Fig. 1) suggests that flood frequencies on the Ohio River were reduced during the MCA and increased during the LIA in response to respective decreases and increases in midcontinental snowpack during these events (Bird et al., 2019). The rationale for these trends was that large fluvial systems like the Ohio River are sensitive to spring snowmelt rather than warm-season rainstorms because only spring snowmelt provides sufficient runoff over a short enough period of time across the entire watershed to generate significant flood discharges (Knox and Daniels, 2002). Warm-season rainstorms, on the other hand, while intense over discrete portions of large watersheds, do not span the entire watershed and hence do not deliver enough precipitation to generate large flood discharges (Knox and Daniels, 2002). Smaller watersheds, however, can be affected by individual rainstorm systems and hence may be susceptible to flooding as a result of discrete rainstorm events (Knox and Daniels, 2002). Previous investigations of watershed responses to precipitation seasonality focused on very small (100s of km^2) or very large (>100,000 km^2) watersheds (Knox and Daniels, 2002). The ways in which intermediate sized watersheds (e.g., 10,000–100,000 km^2) responded to changes in precipitation seasonality, therefore, remains uncertain. Determine the response of intermediately sized fluvial systems to precipitation seasonality and the type of climatic conditions that promote flooding is critical in order to provide a baseline of natural variability against which current fluvial responses to changing precipitation patterns can be gauged.

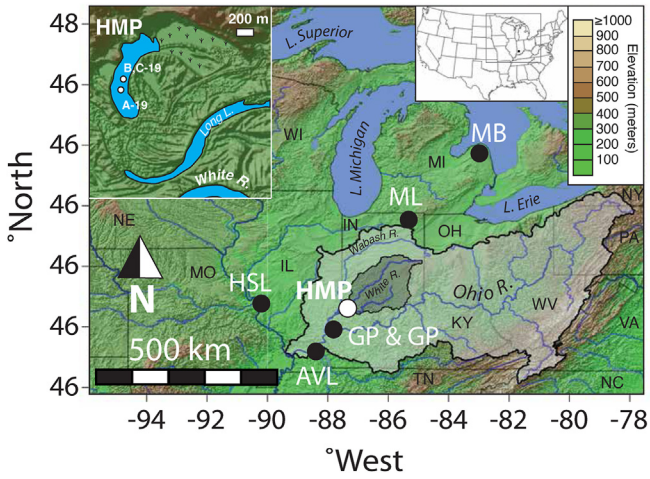

Fig. 1. Digital elevation map of the study area (represented by gray box in the inset map of the United States) showing the watersheds for the Ohio River (light gray shading) and the White River, IN (dark gray shading). Half Moon Pond (HMP) is indicated with a white circle. Black circles indicate published paleoclimate records discussed in the text (HSL = Horseshoe Lake; AVL = Avery Lake; Goose and Grassy ponds = GP & GP; ML = Martin Lake; MB = Minden Bog). Inset map shows an expanded view of Half Moon Pond and its position in the surrounding floodplain (black box in inset map of the United States). Core locations are indicated with white circles.

Here, climate-flood relationships in medium-sized watershed (ca. 29,000 km^2) in the Midwestern United States are investigated using a ca. 1600-year-long lake sediment archive from Half Moon Pond, IN, a small oxbow lake in the lower White River floodplain (Fig. 1). Instrumental stream gauge data demonstrates that flooding on the White River system is sensitive to the occurrence of precipitation events derived from the Gulf of Mexico today, but the long-term stability of this relationship is unknown. To investigate long-term flood frequencies we used sediment accumulation rates and variations in sedimentological and geochemical proxies of clastic flux (i.e., magnetic susceptibility; MS, percent titanium; %Ti, and percent zirconium; %Zr, and grain size analysis) constrained by high-resolution radiocarbon dating. Comparison of these results with regional records for flooding dynamics and climate variability (including atmospheric circulation and precipitation seasonality) illustrates how climate and land-use changes have influenced the flooding regimes of the White River during the last 1600 years and contributes to our understanding of how fluvial systems in the midcontinental US may evolve in response to rapidly changing hydroclimatic conditions.

2. Study area

2.1. Half Moon Pond

Half Moon Pond (N 38.55691, W 87.41694; 124.5 m above sea level) is a 1.25-m-deep oxbow lake on the lower White River in Knox County, IN, approximately 15 km downstream of the confluence of the river's east and west forks near Petersburg, IN (Fig. 1). Half Moon Pond resides on the northern most extent of the approximately 15 km long and 7.5 km wide valley (ca. 2 km wide) (Fig. S1). Combined with the increased flow due to the confluence of the two forks, this geomorphic setting provides ample floodplain within which the White River migrates, as evidenced by the presence of numerous oxbow lakes and paleochannels. The West Fork

has a length of 582 km while the East Fork has a length of 305 km for a total stream length of approximately 887 km (Lane et al., 2017). After the convergence of the two forks, the White River becomes a 7th order stream (McMurray, 2020; Strahler, 1957) with a mean annual discharge of 12,991 ft^3/s at Petersburg, IN (USGS, 2021). The White River subsequently joins the Wabash River at Mt Carmel, IL, which then joins the lower Ohio River near Mt. Vernon, IN.

2.1.1. Regional climate

Like much of the Midwest, the White River valley experiences a humid to humid-subtropical midcontinental climate (Widhalm and Dukes, 2020). Based on 1981–2010 climate norms, average annual temperatures range between 10 and 13 °C with mean maximum temperatures occurring in late July or early August (28–31 °C) and mean minimum temperature in late January or early February (−7 to −4 °C) (Andresen et al., 2012; MRCC, 2021). Precipitation maxima occur in the spring/summer (MAM/JJA) while minima occur in the fall/winter (SON/DJF), with total annual precipitation ranging from 101 to 127 cm (Andresen et al., 2012).

Precipitation is primarily derived from three main sources: the Gulf of Mexico, the Pacific, and the Arctic (Andresen et al., 2012; Bird et al., 2017; Liu et al., 2014). Moisture from the Gulf of Mexico is the greatest contributor to precipitation, with the majority occurring during the warm season when clockwise atmospheric circulation dominates over the eastern United States and draws Gulf moisture deep into the midcontinent (Algarra et al., 2019; Nakamura et al., 2013; Zhang and Villarini, 2019). Advection of moisture from the Gulf of Mexico stimulates mesoscale (ten to several hundred kilometers wide) convective systems, which contribute 30%–70% of warm season precipitation and are responsible for some of the largest floods in the Midwest (Branick et al., 1988; Fritsch et al., 1986; Nakamura et al., 2013). This is in part because warm-season convective storms are frequently comprised of southwest to northeast trending squall lines that can span the width of moderately sized watersheds, like the White River Valley (WRV), thus delivering heavy precipitation across entire watersheds in as little as a few hours.

Extreme precipitation events in the WRV and much of the Midwest are often associated with atmospheric rivers, which are characterized by anomalously strong southwesterly atmospheric flow from Central America and southern Mexico that propagates through the Gulf of Mexico and into the midcontinental US in narrow (~400 km to >1000 km wide) bands (Dirmeyer and Kinter, 2010). Atmospheric rivers are most common in the winter and spring, though they can occur in any season, and are associated with basin-wide flooding in the midcontinental US during any season (Dirmeyer and Kinter, 2010; Lavers and Villarini, 2013; Zhang and Villarini, 2019).

Moisture derived from the North Pacific and Arctic typically falls as snow during the winter, which accounts for ~25% of total annual precipitation (Bird et al., 2017). These polar air masses are transported to the midcontinent by high-amplitude upper tropospheric flow (Andresen et al., 2012). As a result, daily and weekly weather patterns in the winter are mostly influenced by the orientation of the polar jet stream, which drives large-scale midlatitude systems that deliver snow and rain across the region (Andresen et al., 2012; Widhalm and Dukes, 2020).

The proportion of moisture derived from the Gulf of Mexico and the Pacific/Arctic is modulated by variations in large-scale ocean-atmosphere dynamics that are captured by pressure gradients between 1000 and 500 mb levels in the North Pacific that define the Pacific North American Mode (Leathers et al., 1991; Wallace and Gutzler, 1981). During negative Pacific North America (PNA) modes (-PNA), zonal middle tropospheric flow over North America strengthens clockwise air circulation over the eastern half of the US, which advects moisture from the Gulf of Mexico into the midcontinent and generally increases midcontinental rainfall (Coleman and Rogers, 2003; Leathers et al., 1991). Conversely, positive PNA modes (+PNA) feature meridional middle tropospheric flow with a high-pressure atmospheric ridge present over the western US and a low-pressure trough over the eastern US, thereby transporting colder, drier air masses from the northwest and suppressing warmer, wetter air masses from the south, ultimately resulting in a general reduction in midcontinental precipitation. Snowfall, however, is more common during +PNA modes (Serreze et al., 1998).

The PNA is sensitive to conditions in the equatorial Pacific associated with the El Niño-Southern Oscillation (ENSO) such that + ENSO (i.e., El Niño events) is associated with +PNA conditions and -ENSO (i.e., La Niña events) and -PNA modes likewise co-occur (Li et al., 2019; Yu and Zwiers, 2007). On decadal and longer timescales, the PNA is modulated by the Pacific Decadal Oscillation (PDO), which resembles ENSO-like patterns in the North Pacific (Mantua and Hare, 2002). A deepened Aleutian Low over the North Pacific during +PDO phases reinforces + PNA-like atmospheric circulation and hydroclimatic condition whereas a weakened Aleutian Low during -PDO phases contributes to more zonal atmospheric circulation characteristic of -PNA modes (Mantua and Hare, 2002; Rodionov and Assel, 2001).

3. Methods

3.1. Sediment core collection

Two continuous, 5.5-m-long sediment cores (A-19 and B-19) were collected at Half Moon Pond in March 2019 (Fig. 1c; Appx. A). Sediment cores were collected using a modified Livingstone piston corer (Wright et al., 1984) driven by an electric winch coring tower system mounted on a floating raft. To ensure complete recovery, sequential drives were overlapped by 50 cm. The sediment-water interface was captured in an additional 84-cm-long surface core (C-19; Appx. A) using a hand-driven modified piston corer at the B-19 core site. All samples were wrapped in plastic and stored in sealed plastic sleeves at 4 °C at the IUPUI Paleoclimatology and Sedimentology Laboratory prior to analysis.

3.2. Initial sediment characterization and loss on ignition

All cores were split into work and archive halves that were left to equilibrate to room temperature before measuring their magnetic susceptibility (MS; SI $\times 10^{-5}$) using a Bartington MS2 magnetic susceptibility meter powered by a Geotek Multi-Sensor Core Logger. Measurements were made on the split core surface (covered with plastic wrap) at 0.5 cm increments with 2 s per measurement. Due to similarities in stratigraphy and MS trends between cores A-19 and B-19, further analyses were performed solely on a composite core consisting of cores B-19 and C-19.

Following MS analysis, the cores were digitally imaged on the Geotek and then volumetrically subsampled (1 cm^3) at 2-cm intervals for dry bulk density (BD; g cm^{-3}) and loss-on-ignition (LOI) analysis. Samples were dried for 24 h at 60 °C and reweighed for dry BD. Total organic matter (%TOM) and carbonate (%TC) abundances were measured by LOI after sample combustion at 550 °C (4 h) and 1000 °C (2 h), respectively (Boyle, 2000; Heiri et al., 2001). Residual matter (lithics + diatom opal) abundance was calculated by subtracting %TOM and %TC from 100%. Smear slides revealed that diatoms comprised less than 1% of the sediment fraction; therefore, residual matter abundance is effectively percent lithics and may potentially be used as an erosional indicator.

3.3. Age control and accumulation rates

The Half Moon Pond age model is based on 10 radiocarbon (^{14}C) dates of charcoal that were picked from a 63 μm wet sieve after disaggregation in 7% hydrogen peroxide solution for one to 2 min (Fig. 2; Table 1). The samples were physically cleaned and chemically pre-treated following acid-base-acid protocols after Abbott and Stafford (1996) before measurement by accelerator mass spectrometry (AMS) at the Keck AMS Laboratory, University of California, Irvine (UCI). Radiocarbon ages were calibrated to calendar years before present (cal. yr BP; where present = 1950 of the Common Era) using the IntCal20 calibration curve (Reimer et al., 2020). Dates are referred to as being Common Era (CE), unless otherwise stated. The age-depth model and sediment accumulation rates with 2-sigma uncertainties were generated using the Bayesian age modeling software package Bchron (Parnell et al., 2008). Lacustrine sediment accumulation rates were calculated using the Bchron *acc_rate* function, which returns the mean (50%), minimum (2.5%) and maximum (97.5%) accumulation rate estimates for the Bchron age model.

3.4. Grain size analysis

Approximately 1 g of wet sediment was reacted with 35% H_2O_2 (24 h at room temperature followed by 2–3 25 ml aliquots at 70 °C) to remove organic matter and then rinsed with DI water (Gray et al., 2010). Since diatoms were <1% of samples when examined under microscope; the samples were not treated with NaOH. Samples from depths with greater than approximately 4% TC (determined by LOI analysis) were treated with HCl. Grain size measurements were performed using a Malvern Mastersizer 2000 with reported values as the average of three replicate measurements and output parsed into 49 particle size diameter bins between 0.1 and 2000 μm.

3.5. X-ray fluorescence geochemistry

X-ray fluorescence (XRF) analyses provide quick, non-destructive measurements of the total elemental composition of sediments (Boyle, 2000). Using a handheld Olympus Innov-X Delta Pro (DPO-6000-C) XRF analyzer, two energy beams, with a 30 s exposure each, measured the quantity (counts per second) of titanium (Ti) and zirconium (Zr). The results were converted to percent abundance (%) through the XRF system's proprietary software and manufacturer's calibration standard.

3.6. Flux calculations

To express changes in the delivery of clastic material to the lake as a result of inundation, clastic flux was calculated using the bulk density, mean accumulation rates, and %residual as determined by LOI. The flux of clastic material (residual matter) to the lake was derived from:

$$Flux_{clastic} = BD \times AR \times \% \text{ Residual}$$

where *BD* is the dry bulk density (g/cm^3) and *AR* is the mean accumulation rate (cm/yr). Similarly, flux for the sediment constituents Ti and Zr were derived from:

$$Flux_{(Ti,\ Zr)} = BD \times AR \times \text{percent residual matter} \times [(\%Ti, \%Zr)/100]$$

where *BD* is the dry bulk density (g/cm^3) and *AR* is the mean accumulation rate (cm/yr).

4. Results

4.1. Half Moon Pond core stratigraphy

The 545-cm composite Half Moon Pond core was developed by matching visual stratigraphy between overlapping drives. A basal section composed of very fine to coarse sand was visually identified from 545 to 542 cm. This sandy unit is consistent with the composition of modern and paleo-White River channel deposits in this portion of the White River (Herrmann, 2016) and likely reflects White River channel alluvium prior to Half Moon Pond's formation. Above these sands, a sandy silt unit with centimeter-scale layering occurred between 542 and 522 cm. From 522 cm to the top, the core is comprised of brown, fine-grained sediments with little distinct stratigraphy.

4.2. Chronology and sediment accumulation rates

All radiocarbon dates were in stratigraphic order, constraining age-depth relationships. Sediment accumulation rates show three distinct phases (Fig. 2b). Despite large analytical uncertainties (± 190 and 130 years) for two small samples between ca. 330 and 390 cm (UCI #s 245905 and 222133, respectively), bounding ^{14}C ages with small analytical uncertainties (± 15 to 20 years) produced narrow age model uncertainties, increasing the confidence in the age model and subsequent sediment accumulation rate and flux calculations. Accumulation rates increased after the formation of the lake and were generally high to 1100 CE, averaging 0.25 cm/yr, with two distinct peaks from 650 to 830 CE and 1000–1100 CE. Sedimentation rates then decreased from 1100 to 1750 CE, with two minimums from 1150 to 1250 CE and 1500–1660 CE. After 1750 CE, sedimentation rates rebounded dramatically, reaching 1.0 cm/yr by 1930 CE and remaining at record highs to the present.

4.3. Dry bulk density and loss-on-ignition

From 475 to 510 CE, dry BD sharply fell from 1.62 g/cm^3 to 0.83 g/cm^3 (Fig. 2c) as fluvial sands transitioned to lacustrine sediment. Between 510 and 990 CE, dry BD averaged 0.82 g/cm^3, peaking at 1.32 g/cm^3 at 830 CE and decreasing to 0.56 g/cm^3 by 980 CE. Dry BD rose sharply after 1000 CE to 1.28 g/cm^3 by 1150 CE before abruptly decreasing to 0.25 g/cm^3 by 1365 CE. Dry BD recovered to 0.87 g/cm^3 by 1415 CE before decreasing again, reaching 0.26 g/cm^3 at 1760 CE. From 1760 to 1950 CE, dry BD rose to 0.86 g/cm^3 before decreasing to present levels (0.19 g/cm^3 in 2018 CE). Overall, %TOM was antiphased and %residual was in phase with dry BD (Fig. 2d and e). %TC was initially high, reaching a maximum of 11.2% at 465 CE and then decreasing to 2.1% by 1000 CE (Fig. 2f). From 1000 to 1625 CE, %TC remained above 2.1% and below 3.7%. For the remainder of the record (1625 CE to present), % TC varied slightly about a mean of 3.6%.

4.4. Magnetic susceptibility

MS varied considerably throughout the 1600-year Half Moon Pond record (Fig. 3a) From 495 CE to 850 CE, MS fluctuated about a mean of 11.1, reaching 27.3 at 500 CE and 4.3 in 630 CE. By 1045 CE, MS dropped to just 0.1 before gradually increasing to 19.0 in 1390 CE. MS then quickly dropped again to 4.4 by 1420 CE and showed a decreasing trend until 1780 CE. From 1780 CE to the present, MS showed a particularly steep increase that was not featured elsewhere in the record, reaching a maximum of 71.5 in 1950 CE.

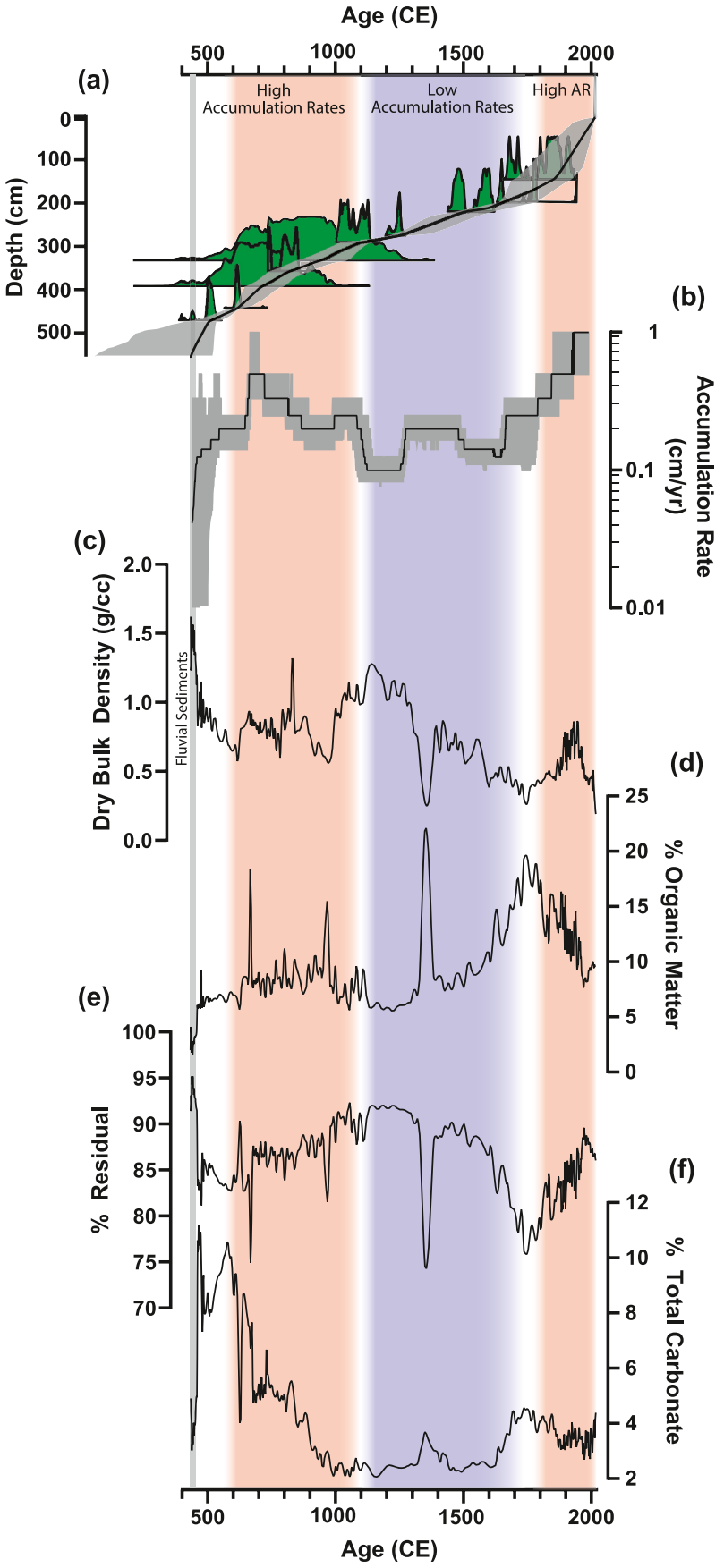
Age (CE)
500
1000
1500
2000
(a)
High Accumulation Rates
Low Accumulation Rates
High AR
Depth (cm)
0
100
200
300
400
500
(b)
Accumulation Rate (cm/yr)
1
0.1
0.01
(c)
Dry Bulk Density (g/cc)
2.0
1.5
1.0
0.5
0.0
Fluvial Sediments
(d)
% Organic Matter
25
20
15
10
5
0
(e)
% Residual
100
95
90
85
80
75
70
(f)
% Total Carbonate
12
10
8
6
4
2
Age (CE)

4.5. Grain size

Silt and clay dominated the grain size distribution, respectively averaging 68.4% and 26.5%, through the record (Fig. 3c and d). Silt abundances were initially low, but quickly rose to 70.3% by 515 CE. Between 515 and 1630 CE, variations in silt were relatively minor, fluctuating by approximately 5.0%. After 1630 CE, silt abundance dropped nearly 24%, falling to 47.4% by 1660 CE. Silt then rose to 65.3% by 1680 CE and showed a decreasing trend from 1680 CE to the present, varying about a mean of 59.0%. Clay abundance generally mirrored that of silt.

Sand was a minor constituent in grain size composition with a mean total abundance of 5.1% (Fig. 3b). Sand was abundant during the fluvial (basal) portion of the core, with a peak of 53.1% at 500 CE. However, sand content dropped considerably after the establishment of a lacustrine environment (ca. 520 CE). Sand content averaged less than 1% until 1650 CE, after which point to the present it averaged 9.0% with several discrete peaks.

4.6. XRF geochemistry

Titanium and Zr abundances showed a strong exponential relationship ($r^2 = 0.83$ $p < 0.001$). Abundances of Ti and Zr were high at the base of the core where fluvial sands dominated and then decreased to minimums at 590 CE (Fig. 4b). For the next ~465 years, Ti and Zr gradually increased to maximums by 975 CE. From 975 to 1370 CE, Ti and Zr remained high before decreases stepwise to lows 1370 CE. A secondary prolonged peak occurred from 1400 to 1580 CE, which was followed by a long decline to minimums in Ti and Zr by 1750 CE. After 1750 CE, Ti and Zr quickly increased again, peaking in 1930 CE.

4.7. Sediment flux

Clastic flux was generally high from 500 to 1120 CE, reaching a maximum of 38.8 g cm^{-2} yr^{-1} at 730 CE (Fig. 4a and c). Clastic flux then remained low (below 15.1 g cm^{-2} yr^{-1}) from 1120 to 1875 CE. From 1875 CE to present, clastic flux quickly increased, reaching a record maximum of 58.6 g cm^{-2} yr^{-1} by 1960 CE. Trends in Ti and Zr fluxes closely tracked changes in clastic flux (Fig. 4c and d).

5. Discussion

5.1. Modern climate-flood relationships at Half Moon Pond

Stream gauge data from Petersburg, IN (USGS station 03374000) that spans 1925–2020 CE indicates that Half Moon Pond is connected to the White River at a stage height of 4.9 m (126.50 m above NAVD88), or a discharge of 29,900 ft^3/s or higher, which has a 1.07-year recurrence interval (USGS, 2021). A more common discharge metric used to assess flood discharges with sufficient magnitude and frequency to conduct geomorphic work is the 1.5-year recurrence interval (RI) discharge (Leopold, 1994). At Petersburg, IN, the 1.5 RI discharge is ca. 60,000 ft^3/s and reaches an elevation of ca. 128.5 m (Fig. S1). The greatest number of days at or above the1.5 RI discharge occurred in January (184), followed by April (154), March (149), May (142), and February (91) (Fig. S1). NCEP-NCAR reanalysis data show that months with the most high discharge days were associated with anomalously strong -PNA-like clockwise atmospheric circulation over the eastern US that advected tropical moisture from the Gulf of Mexico deep into the midcontinent (Figs. S2 and S3) (Kalnay et al., 1996). The nature and timing of these circulation anomalies, i.e., northward advection of Gulf moisture during the winter and spring, are consistent with the occurrence of extreme precipitation events associated atmospheric rivers and other synoptic to mesoscale precipitation bearing systems that are capable of spanning the entirety of the White River watershed (Lavers and Villarini, 2013; Nakamura et al., 2013). In contrast, winter and spring months lacking discharges equal to or greater than the 1.5 RI discharge were characterized by + PNA-like northwesterly atmospheric circulation that suppresses the northward advection of Gulf moisture (Figs. S2 and S3).

Although suspended sediment concentrations were not measured at the Petersburg stream gauge site, a strong positive relationship between stream discharge and suspended sediment in fluvial systems has long been observed (Crawford, 1991; Ferguson, 1986; Toonen et al., 2012). More frequent discharges equal to or greater than the 1.5 RI discharge would therefore be associated with increased sediment delivery to floodplain lakes, like Half Moon Pond, and vice versa for reductions in flood frequency. Given the association between atmospheric circulation that advects moisture from the Gulf and high discharge events on the White River, we suggest that long-term variability in sediment delivery and accumulation at Half Moon Pond reflects the frequency with which Gulf moisture was advected into the Midwest under -PNA-like atmospheric circulation. Snowmelt is still acknowledged as a contributor to high discharges, but these events would occur on average once in the spring whereas Gulf-fed rainstorm events can occur several times a year. More frequent Gulf-fed rainstorms are additionally noted to occur during the winter under -PNA conditions (Coleman and Rogers, 2003), increasing the likelihood of rain-on-snow events that can drive large discharges. The January peak in discharges likely reflects such a response during the instrumental record (Fig. S1). Changes in the frequency of Gulf-fed rainstorm events (during any season) are therefore hypothesized as the primary driver of high discharge events and changes in sediment accumulation over time.

5.2. Late holocene White River flood frequencies

Flood frequencies on the lower White River are inferred from sediment accumulation rates and the flux of clastic material (lithics, Ti, and Zr) to Half Moon Pond (Fig. 4). Generally high sedimentation rates from 500 to 1100 CE (0.20–0.50 cm/yr) with peaks between 520 and 545, 660–750, 830–850, and 990–1100 CE indicates especially pronounced flooding during these times. Clastic, Ti, and Zr fluxes track sedimentation rate trends, supporting greater transport of clastic material to Half Moon Pond as a result of frequent flooding (Fig. 4c and d). Generally decreased sedimentation rates (below 0.25 cm/yr) and clastic flux indicators after 1100 CE suggest less frequent flooding on the White River that persisted until 1790 CE (Fig. 4c and d). Within this timeframe, sedimentation rates increased slightly between 1300 and 1500 CE and 1640–1660 CE, suggesting a slight increase in flooding within this period of overall low flood frequencies. A sharp decrease in clastic, Ti, and Zr fluxes between 1330 and 1390 CE suggests an especially pronounced reduction in White River flooding during this brief interval. Increased sedimentation rates and clastic flux indicators after 1790 CE, and especially after 1860 CE, suggest a return of frequent flooding on the White River. Deforestation and land use changes in

Fig. 2. Plots of (a) age model results with radiocarbon age probability distributions shown in green and the 1-sigma error range indicated by the gray shading, (b) Accumulation rare changes with the 2-sigma eror shown in gray, (c) dry bulk density in g/cc, (d) percent organic matter, (e) percent residual (lithics + biogenic opal), and (f) percent carbonate versus age. Red vertical shading indicates periods of high accumulation rates while blue shading indicates low sedimentation rates.

Table 1
Half Moon Pond radiocarbon age data.

UCI #	Material	Composite depth (cm)	Fraction Modern	Fraction Modern ±	$\Delta^{14}C$ (‰)	Conventional ^{14}C age (BP)	Error ±
222128	Charcoal	143.5	0.9841	0.0017	−15.9	130	15
222129	Charcoal	195	0.9737	0.0017	−26.3	215	15
222131	Charcoal	217.75	0.9565	0.0015	−43.5	355	15
250374	Charcoal	272.5	0.9106	0.0023	−89.4	750	25
222132	Charcoal	287.5	0.8908	0.0015	−109.2	930	15
245905	Charcoal	328.75	0.8690	0.0199	−131.0	1130	190
250375	Charcoal	353.5	0.8637	0.0014	−136.3	1175	15
222133	Charcoal	387.5	0.8496	0.0133	−150.4	1310	130
245906	Charcoal	439	0.8437	0.0019	−156.3	1365	20
222123	Charcoal	467.5	0.8256	0.0014	−174.4	1540	15

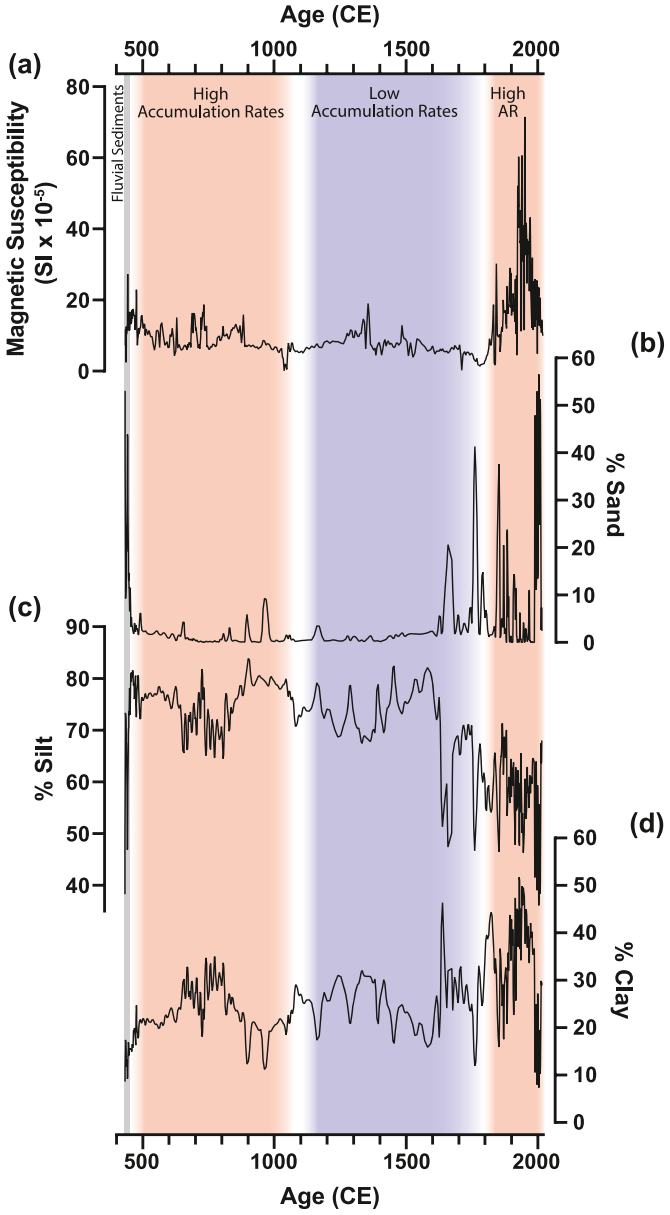

Fig. 3. Plots of (a) magnetic susceptibility in SI $\times 10^{-5}$, (b) percent sand, (c) percent silt, and (d) percent clay versus age. Vertical shading same as in Fig. 2.

1800s and 1900s (Greeley, 1925), however, may have contributed to this signal. Increased % sand after 1700 CE and increased MS after ca. 1800 CE (Fig. 3) may reflect Euro-American landscape impacts given that similar increases in these indicators didn't occur during the MCA when sedimentation rates were elevated, but the landscape was forested. Decreases in clastic, Ti, and Zr fluxes in the upper few centimeters of the Half Moon Pond sediment archive are interpreted to reflect decreases in sediment compaction and high water content, which is common in recently deposited lacustrine sediment that has not undergone natural compaction as a result of subsequent sediment accumulation. As such, decreases in clastic, Ti, and Zr fluxes in the upper few cm of the sediment archive are not interpreted to indicate reduced flooding, but merely to reflect sediment depositional processes.

5.3. Late holocene climate-flood frequency relationships

To evaluate the connections between White River flood frequencies and paleoclimatic conditions, we compared the Half Moon Pond data with a suite of high-resolution paleoclimate proxies from Martin Lake, IN (Fig. 5a–d) (Bird et al., 2017). The oxygen isotopic composition of authigenic calcite ($\delta^{18}O_{cal}$) at Martin Lake has been shown to reflect the annual average $\delta^{18}O$ of precipitation ($\delta^{18}O_{precip}$), which in turn is controlled by the advection of moisture from two primary sources via PNA-like synoptic-scale atmospheric circulation (Fig. 5d) (Bird et al., 2017; Liu et al., 2014). High $\delta^{18}O_{cal}$ values are associated with moisture originating from the Gulf of Mexico (ca. −5.5‰), typically during the warm season, that is advected into the North American midcontinent by -PNA-like atmospheric circulation. Conversely, low $\delta^{18}O_{cal}$ values (ca. −16.5‰) reflect moisture sourced from the North Pacific/Arctic that is advected into the North American midcontinent by + PNA-like conditions, most commonly during the cold season (Bird et al., 2017; Liu et al., 2014). Watershed-scale runoff and erosion due to warm-season rainstorm events were reconstructed at Martin Lake using % lithics, whereby elevated %lithics reflects increased warm-season rainstorm events and water shed erosion and vice versa for decreases (Fig. 5c).

When compared with the Half Moon Pond sedimentation rates and clastic flux indicators, the Martin Lake data shows that flood frequencies increased when $\delta^{18}O_{cal}$ and %lithics were elevated and decreased when $\delta^{18}O_{cal}$ and %lithics were low (Fig. 5). The agreement between these records is best between 500 and 1350 CE and after 1820 CE with subtle offsets between 1350 and 1820 CE. These offsets however occur within the portion of the Half Moon Pond record that has limited age control, and hence greater age range uncertainty, because of a paucity of charcoal for dating. Low charcoal abundances may reflect less landscape burning because of cooler and shorter warm seasons during the LIA, but it is also possible that decreasing indigenous populations in Indiana during the LIA (Milner et al., 2001; Monaghan et al., 2013) resulted in reduced landscape burning and hence lower charcoal fluxes during this time. Taking age model uncertainty into account and the otherwise good inter-record agreement, it is possible that maxima

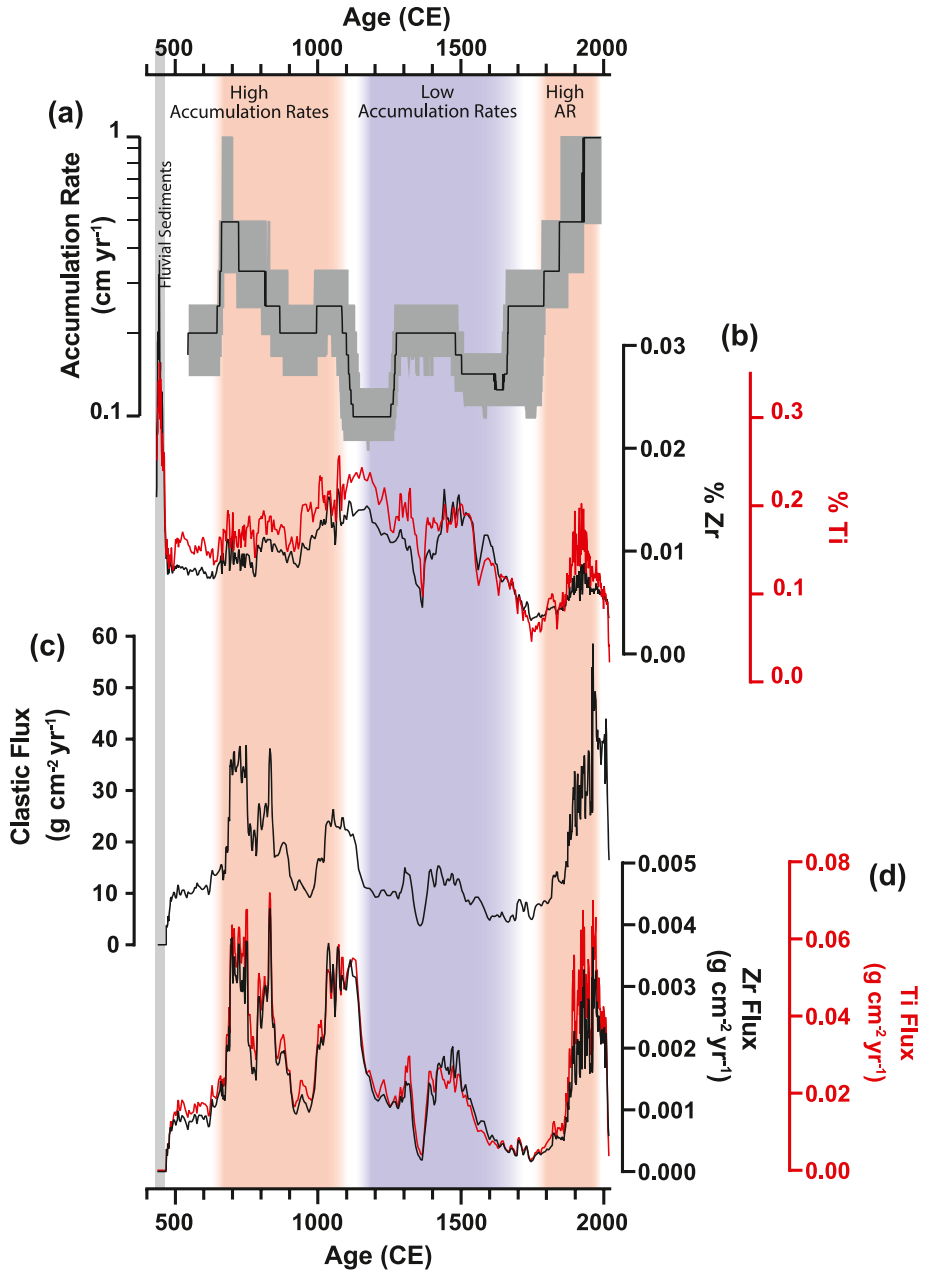

Fig. 4. Comparison of (a) sediment accumulation rates in cm^{-1} with (b) percent zirconium (Zr) and titanium (Ti), (c) clastic flux in g cm^{-2} yr^{-1}, (d) and Zr and Ti fluxes in g cm^{-2} yr^{-1} versus age. Vertical shading same as in previous figures.

and minima in the Half Moon Pond clastic flux records and Martin Lake $\delta^{18}O_{cal}$ and %lithics records between 1350 and 1820 CE were contemporaneous. However, other climatic possibilities are also considered below. Regardless, the generally in-phase relationship between the Half Moon Pond clastic flux indicators and Martin Lake $\delta^{18}O_{cal}$ and %lithics hydroclimate proxies supports our contention that White River flood frequencies increased at times in the past when -PNA-like atmospheric circulation advected moisture from the Gulf of Mexico during extended warm-season conditions and decreased when + PNA-like ridge and trough atmospheric circulation blocked Gulf moisture and enhanced moisture delivery from the Pacific/Arctic, most likely in the form of snow (Serreze et al., 1998), during extended cold seasons.

The relationship between White River flood frequencies and PNA-like synoptic-scale atmospheric circulation is consistent with records of ocean-atmosphere processes spanning the last 1600 years. Specifically, the concurrence of -PNA-like atmospheric circulation and increased White River flood frequencies between 500 and 1100 CE occurred when the North Pacific was in a predominantly -PDO-like mean state and -ENSO-like (La Niña-like) conditions prevailed in the tropical Pacific (Fig. 5) (Mann et al., 2009; Seager et al., 2007). Especially pronounced -PDO and -PNA conditions and increased White River flood frequencies occurred during the MCA (Mann et al., 2009; Seager et al., 2007), a period that has been noted as a time of increased warm-season precipitation and effective moisture across the Midwest east of ca. 96° W (Bird et al., 2017; Booth et al., 2006; Pompeani et al., 2021; Tian et al., 2006) when regional and Northern Hemisphere temperatures were also warm (Fig. 5) (Mann et al., 2009; Viau et al., 2006).

The transition to reduced White River flooding and +PNA-like

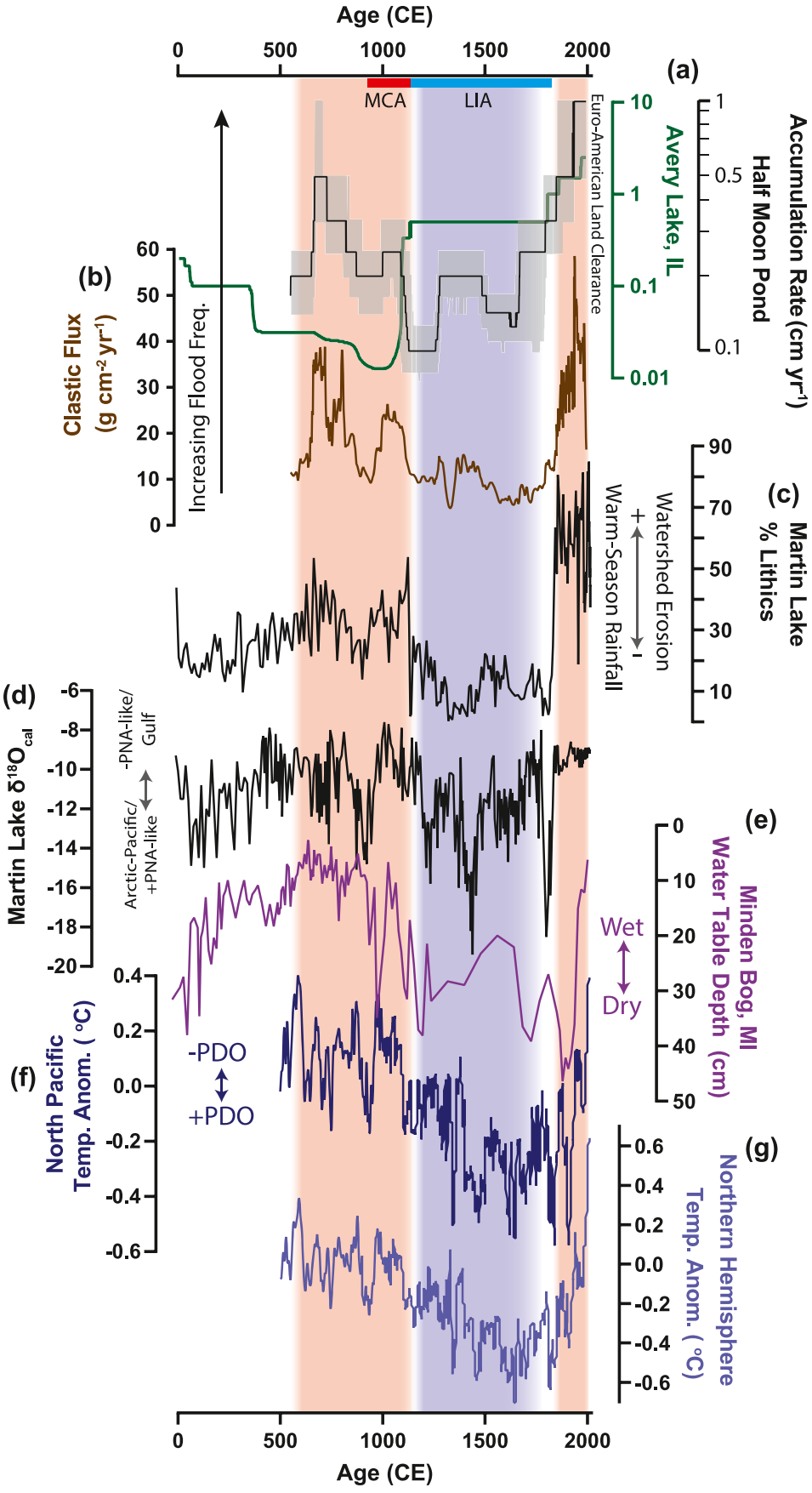
Age (CE)
0
500
1000
1500
2000
(a)
MCA
LIA
Euro-American Land Clearance
Avery Lake, IL
10
1
0.1
0.01
Half Moon Pond
1
0.5
0.1
Accumulation Rate (cm yr-1)
(b)
Clastic Flux
(g cm-2 yr-1)
60
50
40
30
20
10
0
Increasing Flood Freq.
(c)
Martin Lake
% Lithics
90
70
50
30
10
Watershed Erosion
Warm-Season Rainfall
+
-
(d)
Martin Lake δ18Ocal
-6
-8
-10
-12
-14
-16
-18
-20
-PNA-like/
Gulf
Arctic-Pacific/
+PNA-like
(e)
Minden Bog, MI
Water Table Depth (cm)
0
10
20
30
40
50
Wet
Dry
(f)
North Pacific
Temp. Anom. (°C)
0.4
0.2
0.0
-0.2
-0.4
-0.6
-PDO
+PDO
(g)
Northern Hemisphere
Temp. Anom. (°C)
0.6
0.4
0.2
0.0
-0.2
-0.4
-0.6
0
500
1000
1500
2000
Age (CE)

atmospheric circulation between 1100 and 1130 CE coincided with the transition to + PDO and +ENSO conditions during the transition to the LIA (Bird et al., 2017) as regional and Northern Hemisphere temperatures also cooled (Mann et al., 2009; Viau et al., 2006) (Fig. 5). Generally reduced White River flooding during the LIA is consistent with +PNA, +PDO and +ENSO-like conditions that tend to reduce precipitation overall in midcontinental North America and the Ohio River Valley in particular (Coleman and Rogers, 2003). Within the LIA, increased White River flooding between ca. 1380–1515 CE when $^{18}O_{cal}$ and %lithics at Martin Lake were low (strong + PNA-like conditions) and the PDO was in a strong positive phase contrasts with the otherwise in-phase climate flood relationships during the last ca. 1600 years. Although age model uncertainties may contribute to this apparent misalignment between White River flood frequencies and PNA and PDO variability between 1380 and 1515 CE, it is also possible that these trends reflect a slight increase in flooding due to greater snowpack during the LIA. Given that strong + PNA phases increase snowfall in the Midwest today (Serreze et al., 1998), it is possible that exceptionally heavy snowfall between 1380 and 1515 CE (minima $\delta^{18}O_{cal}$ at Martin Lake) resulted in large spring snowmelt events. That increased runoff is not indicated by the Martin Lake %lithics record is in line with observational studies that found fluvial systems in small watersheds are not particularly sensitive to spring snow melt-driven flooding (Knox and Daniels, 2002). With a watershed area of 125 km^2, runoff to Martin Lake is therefore unlikely to be affected by snowmelt runoff even under heavy snowpack conditions. With a watershed size of ~29,000 km^2, however, the White River is likely to be influenced by both rainstorm and snowmelt runoff, though, as discussed above, the frequency of rainstorm events is likely the primary driver. In the absence of significant warm-season rainstorm precipitation and during a time of enhanced snowpack, such as between 1380 and 1515 CE, it is possible that spring snow melt was sufficient to generate flooding during this interval. Another possibility is that strong cold-season-like conditions during this time, as indicated by minimum $\delta^{18}O_{cal}$ at Martin Lake, resulted in more frequent ice jams. Large modern floods in the Midwest have been linked to ice jams (Carr and Vuyovich, 2014), and while their long-term occurrence is not known and difficult to constrain, it is possible that they may have contributed to the slightly increased flood frequencies between 1380 and 1515 CE. Regardless, sediment accumulation rates and clastic flux indicators show that White River flood frequencies during this period were lower than during the MCA.

Increased White River flooding after 1790 CE coincided with the transition to the CWP when the Martin Lake record indicates that -PNA-like atmospheric circulation again predominated (Fig. 5). Sedimentation rates at Half Moon Pond, however, increased by ca. 400% to levels not achieved in the last 1600 years. While increased White River flood frequencies during the CWP are consistent with climate-flood relationships during the MCA, the magnitude of the sedimentation rate increase suggests that additional factors may be at play. Deforestation and the conversion of forest to agricultural and pastureland in the White River drainage basin during the 1800s and 1900s are likely contributors because they serve to reduce infiltration and evapotranspiration, thereby increasing runoff and stream discharge. Additional factors that contribute to increased discharge are agricultural tiling, which is pervasive throughout Indiana, and the construction of levees that disconnect streams from their floodplains, which increases peak storm discharge. It is possible that the onset of high %sand at Half Moon Pond at 1650 CE and intensification after 1800 CE reflects the influence of deforestation and land use change on the intensity of floods occurring on the White River. Therefore, while the current state of frequent White River flooding is consistent with paleo climate-flood relationships, it is likely that anthropogenic activities have contributed to the unprecedented nature of current flood frequencies and possibility intensities.

5.4. Regional climate-flood relationships and watershed scale

Modern observations of fluvial systems indicate flooding on streams with large watersheds (>100,000 km^2; e.g., the Missouri, Mississippi, Ohio Rivers) is controlled by the spring snowmelt whereas flooding on streams with small watersheds (100's km^2 or less) is sensitive to the occurrence of rainstorm events (Knox and Daniels, 2002). This is because meteorological systems that produce intense rainfall events are not large enough to cover the entire watershed of large streams and thus do not result in sufficient basin-wide runoff to regularly generate flood events. In contrast, the spring snowpack melt, which can represent the accumulation of several months' worth of precipitation events, produces sufficient basin-wide runoff to generate flooding on large streams. Meteorological systems that produce extreme rainfall, however, are of sufficient size to cover small watersheds, and hence are capable of driving rainstorm-driven flooding. Whether or not these relationships were similar in the past and at what size watersheds transition from being rainstorm-sensitive to snowmelt-sensitive with respect to flooding remains unknown.

The similarities between the Half Moon Pond clastic flux indicators and Martin Lake %lithics indicates that the lower White River with a watershed size of ca. 29,000 km^2 (represented by Half Moon Pond) and the headwaters of the East Fork Elkhart River with a watershed size of 125 km^2 (represented by Martin Lake) were both sensitive to the frequency and occurrence of rainfall events during at least the last 1600 years. Although the White River was also potentially influenced by snowpack melt during the height of the LIA between 1380 and 1515 CE, flood frequencies were on average reduced during the LIA because of less frequent incursions of moisture from the Gulf of Mexico. The Martin Lake and Half Moon Pond records are additionally consistent with other regional hydroclimate records from Minden Bog, MI (Booth et al., 2006), and Horseshoe Lake, IL (Pompeani et al., 2021). These records respectively indicate elevated water tables (Fig. 5e) and increased effective during the MCA when flood frequencies at Half Moon Pond and runoff from warm-season rainstorm events at Martin Lake were increased. Together, these data indicate a consistent regional response to hydroclimate conditions during the Common Era.

At the other end of the watershed size spectrum are sedimentation-rate-based records of lower Ohio River flood frequencies from Avery Lake, IL, Goose Pond, IN, and Grassy Pond, IN, which reflect climate-flood dynamics for a ca. 530,000 km^2 watershed (Fig. 5b) (Bird et al., 2019; Gibson et al., 2022 In Review). Comparison of the longest continuous record of lower Ohio River flooding from Avery Lake with the Half Moon Pond sediment accumulation record shows they were anti-phased during the LIA, MCA, and before, but in-phase during the CWP. Anti-phasing during and prior to the MCA is consistent with a reduced cold-season snowpack and increased warm-season rainfall that would respectively reduce flooding on the large river systems like the Ohio River

Fig. 5. Comparison of (a) Avery Lake (green line; error shading not included for clarity) and Half Moon Pond (black line) accumulation rates with (b) Half Moon Pond clastic flux rates, (c) Martin Lake percent lithics, (d) Martin Lake $\delta^{18}O_{cal}$, (e) Minden Bog depth to water table, (f) North Pacific sea surface temperature anomalies, and (g) Northern Hemisphere surface temperature anomalies. Vertical shading same as in previous figures. The local timing of the MCA (red line) and LIA (blue line) are additionally indicated.

and increase it in smaller watersheds, like the White River and at Martin Lake (Fig. 5). The shift to increased flooding on the Ohio River and decreased flooding in the White River and Martin Lake (i.e., upper Elkhart River) watersheds during the LIA is consistent with the impact that increased snowpack and reduced warm-season rainfall during the LIA would have on flooding and erosion in respectively large and "small" watersheds.

Increased sedimentation rates on the White River during the CWP are consistent with its response leading up to and during the MCA, albeit at a much higher magnitude because of anthropogenic factors. Increased sedimentation rates at Avery Lake, however, reflect more frequent flooding during climatic conditions that in the past (i.e., the MCA) reduced flooding (Bird et al., 2017, 2019). This departure from "natural" climate-flood relations has been attributed to increases in runoff and erosion because of extensive, large-scale deforestation and land use changes that occurred in the Ohio River watershed and across the eastern US during the Euro-American periods from the 1700s–1900s (Bird et al., 2019; Commerford et al., 2022; Greeley, 1925). Given that the majority of Ohio River flood events over the last ca. 100 years still occurred during the winter/spring months, the increase in CWP flood frequencies suggests that anthropogenic land use modifications have expedited the transit of snowmelt through its watershed, making it more sensitive to snowmelt and winter/spring rain on snow events that are associated with many high discharge events during the instrumental period (Schlef et al., 2018). Were the Ohio River watershed landscape in its pre-Euro-American state today, it is unlikely that CWP climatic conditions would result in the present degree of flooding.

Similar increases in flood indicators at Avery Lake, Half Moon Pond, and Martin Lake demonstrates that fluvial geomorphic responses to Euro-American land use were consistent across watershed scales. Although additional work is needed to determine if flood frequencies in other moderately sized Midwestern watersheds (100,000 $\geq$ 10,000 km^2) tracked those of the White River, coherent increases in the duration and frequency of Midwestern floods during recent decades suggests that midcontinental streams are similarly sensitive to mean annual precipitation and the frequency of heavy rainstorm events. With predicted to increases in midcontinental precipitation and extreme events (Easterling et al., 2017), flooding and geomorphic adjustments are likely to follow.

6. Conclusions

Half Moon Pond sedimentation rates and clastic flux indicators reflect the frequency of flooding on the White River, IN. Frequent flooding leading up to and during the MCA and CWP were the result of -PNA-like atmospheric circulation that advected moisture from the Gulf of Mexico deep into midcontinental North America, producing substantial rainfall (likely during all seasons) that drove increased runoff and stream discharge. Deforestation and land use in addition to a return to -PNA/-PDO-like conditions during the CWP increased the fluvial geomorphic response to rainstorm events, leading to greater flooding and landscape erosion than any other time in the last 1600 yeas. Reductions in White River flood frequencies during the LIA reflect + PNA/+PDO-like conditions that decreased rainfall and increase in snowfall, which reduced runoff and stream discharge. White River flood frequencies during the MCA and LIA were anti-phased with those of the Ohio River. This is consistent with their respective watershed-scale responses to -PNA/-PDO-like conditions during the MCA, i.e., increased warm-season-like conditions with ample rainfall and reduced snowfall, and +PNA/+PDO-like conditions during the LIA, i.e., cold-season-like conditions with increased snowfall and reduced rainfall. The shift to increased sedimentation rates on the White and Ohio rivers during the CWP reflects an amplification of expected conditions on the White River under -PNA-like conditions, but a departure from "natural" climate-flood relationships for the Ohio River. Increased Ohio River flooding during the CWP is consistent with the more rapid transport of runoff through its drainage system due to deforestation, urbanization, agriculturalization, and flood plain disconnectivity and subsequent increase in peak flood stage discharge. Given generally -PNA-like conditions today, it is unlikely that the Ohio River would exhibit it current flood frequency were its watershed in a "natural" state. Within the context of our presently altered landscape and projected increases in mean annual precipitation and heavy rainfall events, it is likely that fluvial system spanning all spatial scales will experience increased flooding in coming decades.

Author contributions

Maxwell Wright: Conceptualization, Investigation, Methodology, Writing, Broxton W. Bird: Conceptualization, Investigation, Methodology, Resources, Writing, Visualization, Supervision, Funding acquisition, Derek K. Gibson: Investigation, Methodology, Writing, Harvie Pollard: Investigation, Writing, Jaime Escobar: Investigation, Writing, Robert C. Barr: Investigation, Conceptualization, Writing.

Declaration of competing interest

The authors declare that they have no known competing financial interests or personal relationships that could have appeared to influence the work reported in this paper.

Data availability

All original data presented in this manuscript are available at the NOAA/WDS paleoclimate data archive: https://www.ncei.noaa.gov/access/paleo-search/study/37163

Acknowledgements

Financial support for this research was provided by the National Science Foundation (EAR 1903628), The Nature Conservancy (Award 2041–0002), and The Indiana Department of Natural Resources, (award 34068).

Appendix A. Supplementary data

Supplementary data to this article can be found online at https://doi.org/10.1016/j.quascirev.2022.107939.

References

Abbott, M.B., Stafford, T.W., 1996. Radiocarbon geochemistry of modern and ancient Arctic lake systems, Baffin Island, Canada. Quat. Res. 45, 300–311.
Algarra, I., Eiras-Barca, J., Miguez-Macho, G., Nieto, R., Gimeno, L., 2019. On the assessment of the moisture transport by the Great Plains low-level jet. Earth System Dynamics 10, 107–119.
Andresen, J., Hilberg, S., Kunkel, K., Center, M.R.C., 2012. Historical Climate and Climate Trends in the Midwestern USA. US National Climate Assessment Midwest Technical Input Report, pp. 1–18.
Bird, B.W., Barr, R.C., Commerford, J., Gilhooly III, W.P., Wilson, J.J., Finney, B., McLauchlan, K., Monaghan, G.W., 2019. Late-Holocene floodplain development, land-use, and hydroclimate–flood relationships on the lower Ohio River, US. Holocene 29, 1856–1870.
Bird, B.W., Wilson, J.J., Gilhooly III, W.P., Steinman, B.A., Stamps, L., 2017. Midcontinental Native American population dynamics and late Holocene hydroclimate extremes. Sci. Rep. 7, 41628.
Booth, R.K., Notaro, M., Jackson, S.T., Kutzbach, J.E., 2006. Widespread drought episodes in the western Great Lakes region during the past 2000 years: geographic extent and potential mechanisms. Earth Planet Sci. Lett. 242,

415–427.
Boyle, J.F., 2000. Rapid elemental analysis of sediment samples by isotope source XRF. J. Paleolimnol. 23, 213–221.
Branick, M.L., Vitale, F., Lai, C.-C., Bosart, L.F., 1988. The synoptic and subsynoptic structure of a long-lived severe convective system. Mon. Weather Rev. 116, 1335–1370.
Coleman, J.S., Rogers, J.C., 2003. Ohio River Valley winter moisture conditions associated with the Pacific-North American teleconnection pattern. J. Clim. 16, 969–981.
Commerford, J.L., Gittens, G., Gainforth, S., Wilson, J.J., Bird, B.W., 2022. Differences in forest composition following two periods of settlement by pre-Columbian Native Americans. Veg. Hist. Archaeobotany 1–14.
Crawford, C.G., 1991. Estimation of suspended-sediment rating curves and mean suspended-sediment loads. J. Hydrol. 129, 331–348.
Dirmeyer, P.A., Kinter III, J.L., 2010. Floods over the US Midwest: a regional water cycle perspective. J. Hydrometeorol. 11, 1172–1181.
Easterling, D.R., Kunkel, K., Arnold, J., 2017. Precipitation Change in the United States.
Ferguson, R., 1986. River loads underestimated by rating curves. Water Resour. Res. 22, 74–76.
Fritsch, J., Kane, R., Chelius, C., 1986. The contribution of mesoscale convective weather systems to the warm-season precipitation in the United States. J. Appl. Meteorol. Climatol. 25, 1333–1345.
Gibson, D.K., Bird, B.W., Pollard, H.J., Barr, R.C., Escobar, J., 2022. Using sediment accumulation rates in floodplain paleochannel lakes to reconstruct climate-flood relationships on the lower Ohio River. In Review Quat. Sci. Rev.
Gray, A.B., Pasternack, G.B., Watson, E.B., 2010. Hydrogen peroxide treatment effects on the particle size distribution of alluvial and marsh sediments. Holocene 20, 293–301.
Greeley, W.B., 1925. The relation of geography to timber supply. Econ. Geogr. 1, 1–14.
Herrmann, E.W., 2016. How bedrock-controlled channel migration can structure selective preservation of archaeological sites: implications for modeling paleoindian settlement. Geoarchaeology 31, 58–74.
Kalnay, E., Kanamitsu, M., Kistler, R., Collins, W., Deaven, D., Gandin, L., Iredell, M., Saha, S., White, G., Woollen, J., 1996. The NCEP/NCAR 40-year reanalysis project. Bull. Am. Meteorol. Soc. 77, 437–472.
Knox, J.C., Daniels, J.M., 2002. Watershed Scale and the Stratigraphic Record of Large Floods. Ancient Floods, Modern Hazards, pp. 237–255.
Lane, C., Hall, A., D'Amico, E., Sangwan, N., Merwade, V., 2017. Characterizing the extent of spatially integrated floodplain and wetland systems in the White River, Indiana, USA. JAWRA Journal of the American Water Resources Association 53, 774–790.
Lavers, D.A., Villarini, G., 2013. Atmospheric rivers and flooding over the central United States. J. Clim. 26, 7829–7836.
Leathers, D.J., Yarnel, B., Plalecki, M.A., 1991. The Pacific/North American teleconnection pattern and the United States climate. Part I: regional temperature and precipitation associations. J. Clim. 4, 517–528.
Leopold, L.B., 1994. A View of the River. Harvard University Press.
Li, X., Hu, Z.-Z., Liang, P., Zhu, J., 2019. Contrastive influence of ENSO and PNA on variability and predictability of North American winter precipitation. J. Clim. 32, 6271–6284.
Lins, H.F., 2012. USGS Hydro-Climatic Data Network 2009 (HCDN-2009), vol. 3047. US Geological Survey Fact Sheet.
Liu, Z., Yoshmura, K., Bowen, G.J., Welker, J.M., 2014. Pacific–North American teleconnection controls on precipitation isotopes ($\delta^{18}O$) across the contiguous United States and adjacent regions: a GCM-based analysis. J. Clim. 27, 1046–1061.
Mallakpour, I., Villarini, G., 2015. The changing nature of flooding across the central United States. Nat. Clim. Change 5, 250–254.
Mann, M.E., Zhang, Z., Rutherford, S., Bradley, R.S., Hughes, M.K., Shindell, D., Ammann, C., Faluvegi, G., Ni, F., 2009. Global signatures and dynamical origins of the little ice age and medieval climate anomaly. Science 326, 1256–1260.
Mantua, N.J., Hare, S.R., 2002. The pacific decadal oscillation. J. Oceanogr. 58, 35–44.
McMurray, P.D., 2020. 2020 Probabilistic Monitoring Work Plan for the West Fork and Lower White River Basin.
Milner, G.R., Anderson, D.G., Smith, M.T., 2001. The Distribution of Eastern Woodlands Peoples at the Prehistoric and Historic Interface. Smithsonian Institution Press, Washington, D.C.
Monaghan, G.W., Schilling, T., Krus, A.M., Peebles, C.S., 2013. Mound construction chronology at angel mounds episodic mound construction and ceremonial events. Midcont. J. Archaeol. 38, 155–170.
MRCC, M.R.C.C., 2021. Climate Trends Tool online at. https://mrcc.purdue.edu/mw_climate/climateTrends.jsp.
Nakamura, J., Lall, U., Kushnir, Y., Robertson, A.W., Seager, R., 2013. Dynamical structure of extreme floods in the US Midwest and the United Kingdom. J. Hydrometeorol. 14, 485–504.
Parnell, A.C., Haslett, J., Allen, J.R., Buck, C.E., Huntley, B., 2008. A flexible approach to assessing synchroneity of past events using Bayesian reconstructions of sedimentation history. Quat. Sci. Rev. 27, 1872–1885.
Pompeani, D., Bird, B.W., Wilson, J.J., Abbott, M.B., Finkenbinder, M.S., Hillman, A.L., 2021. Severe little ice age drought in the midcontinental United States during the mississippian abandonment of cahokia. Sci. Rep. 11, 1–8.
Reimer, P.J., Austin, W.E., Bard, E., Bayliss, A., Blackwell, P.G., Ramsey, C.B., Butzin, M., Cheng, H., Edwards, R.L., Friedrich, M., 2020. The IntCal20 Northern Hemisphere radiocarbon age calibration curve (0–55 cal kBP). Radiocarbon 62, 725–757.
Rodionov, S., Assel, R., 2001. A new look at the Pacific/North American index. Geophys. Res. Lett. 28, 1519–1522.
Schlef, K.E., Francois, B., Robertson, A.W., Brown, C., 2018. A general methodology for climate-informed approaches to long-term flood projection—illustrated with the Ohio river basin. Water Resour. Res. 54, 9321–9341.
Seager, R., Graham, N., Herweijer, C., Gordon, A., Kushnir, Y., Cook, E., 2007. Blueprints for medieval hydroclimate. Quat. Sci. Rev. 26, 2322–2336.
Serreze, M.C., Clark, M.P., McGinnis, D.L., Robinson, D.A., 1998. Characteristics of snowfall over the eastern half of the United States and relationships with principal modes of low-frequency atmospheric variability. J. Clim. 11, 234–250.
Slack, J.R., Lumb, A.M., Landwehr, J.M., 1993. Hydro-climatic Data Network (HCDN): Streamflow Data Set, pp. 1874–1988.
Strahler, A.N., 1957. Quantitative analysis of watershed geomorphology. Eos, Transactions American Geophysical Union 38, 913–920.
Tian, J., Nelson, D.M., Hu, F.S., 2006. Possible linkages of late-Holocene drought in the North American midcontinent to Pacific Decadal Oscillation and solar activity. Geophys. Res. Lett. 33.
Toonen, W.H., Kleinhans, M.G., Cohen, K.M., 2012. Sedimentary architecture of abandoned channel fills. Earth Surf. Process. Landforms 37, 459–472.
USGS, 2021. Water Data, online at. https://waterdata.usgs.gov.
Viau, A., Gajewski, K., Sawada, M., Fines, P., 2006. Millennial-scale temperature variations in North America during the Holocene. J. Geophys. Res. Atmos. 111.
Wallace, J.M., Gutzler, D.S., 1981. Teleconnections in the geopotential height field during the Northern Hemisphere winter. Mon. Weather Rev. 109, 784–812.
Widhalm, M., Dukes, J.S., 2020. Introduction to the Indiana climate change impacts assessment: overview of the process and context. Climatic Change 163, 1869–1879.
Wright, H.E., Mann, D.H., Glaser, P.H., 1984. Piston corers for peat and lake sediments. Ecology 65, 657–659.
Xiao, Y., Wan, J., Hewings, G.J., 2013. Flooding and the Midwest economy: assessing the Midwest floods of 1993 and 2008. Geojournal 78, 245–258.
Yu, B., Zwiers, F.W., 2007. The impact of combined ENSO and PDO on the PNA climate: a 1,000-year climate modeling study. Clim. Dynam. 29, 837–851.
Zhang, W., Villarini, G., 2019. On the weather types that shape the precipitation patterns across the US Midwest. Clim. Dynam. 53, 4217–4232.